

Cluster Cosmology with the Velocity Distribution Function of the HeCS-SZ Sample

MICHELLE NTAMPAKA,^{1,2} KEN RINES,³ AND HY TRAC⁴

¹*Center for Astrophysics | Harvard & Smithsonian, Cambridge, MA 02138, USA*

²*Harvard Data Science Initiative, Harvard University, Cambridge, MA 02138, USA*

³*Department of Physics & Astronomy, Western Washington University, Bellingham, WA 98225, USA*

⁴*McWilliams Center for Cosmology, Department of Physics, Carnegie Mellon University, Pittsburgh, PA 15213, USA*

ABSTRACT

We apply the Velocity Distribution Function (VDF) to a sample of Sunyaev-Zel'dovich (SZ)-selected clusters, and we report preliminary cosmological constraints in the σ_8 - Ω_m cosmological parameter space. The VDF is a forward-modeled test statistic that can be used to constrain cosmological models directly from galaxy cluster dynamical observations. The method was introduced in [Ntampaka et al. \(2017\)](#) and employs line-of-sight velocity measurements to directly constrain cosmological parameters; it is less sensitive to measurement error than a standard halo mass function approach. The method is applied to the Hectospec Survey of Sunyaev-Zeldovich-Selected Clusters (HeCS-SZ) sample, which is a spectroscopic follow up of a *Planck*-selected sample of 83 galaxy clusters. Credible regions are calculated by comparing the VDF of the observed cluster sample to that of mock observations, yielding $\mathcal{S}_8 \equiv \sigma_8 (\Omega_m/0.3)^{0.25} = 0.751 \pm 0.037$. These constraints are in tension with the *Planck* Cosmic Microwave Background (CMB) TT fiducial value, which lies outside of our 95% credible region, but are in agreement with some recent analyses of large scale structure that observe fewer massive clusters than are predicted by the *Planck* fiducial cosmological parameters.

Keywords: cosmology: cosmological parameters — galaxies: clusters: general — methods: statistical

1. INTRODUCTION

Galaxy clusters are massive, gravitationally bound collections of hundreds to thousands of galaxies. The standard cosmological model predicts that the abundance of clusters as a function of their mass and redshift depends sensitively on the underlying cosmological parameters. Because cluster counts depend on the cosmological model, cluster abundance measurements can be used to put constraints on cosmological parameters such as the amplitude of matter fluctuations, σ_8 , and the matter density parameter, Ω_m (e.g. [Bahcall & Fan 1998](#)). More recently, forward-modeling approaches have been used to describe cluster abundance, not by the cluster counts as a function of mass and redshift, but by the distribution of direct observables (e.g. [Wilson et al. 2012](#); [Hill et al. 2014](#); [Caldwell et al. 2016](#); [Pierre et al. 2017](#); [Ntampaka et al. 2017](#)). Forward-modeling approaches can minimize biases that would otherwise be introduced by mass measurement error and can provide

a complementary and mass-independent way to evaluate the abundance of clusters.

Cluster abundance and other large scale structure (LSS) measurements can be used to constrain cosmological models, but some current LSS data are in tension with *Planck* CMB constraints of cosmological parameters. Notably, SZ surveys find fewer massive clusters than are predicted by the *Planck* CMB fiducial cosmology (e.g. [Planck Collaboration et al. 2016b](#)); one interpretation of this is that the *Planck* SZ survey prefers a σ_8 lower than the CMB fiducial cosmology. While some LSS probes are consistent with *Planck* constraints (e.g. [Mantz et al. 2015](#)), others prefer a low σ_8 (e.g. [Heymans et al. 2013](#); [Hildebrandt et al. 2017](#)). In a rigorous analysis of WiggleZ, SDSS RSD, CFHTLenS, CMB lensing and SZ cluster count by [Lin & Ishak \(2017\)](#), these LSS probes are found to be inconsistent with *Planck* CMB cosmological constraints. This tension may be due to unaccounted systematic errors or it may be indicative of more interesting physics that needs to be included in the model.

A number of explanations have been suggested to resolve this tension. X-ray cluster mass measurements un-

der the assumption of hydrostatic equilibrium can incorporate nonthermal pressure support in the form of a bias parameter, b , that relates the SZ mass to the true cluster mass, $M_{\text{SZ}} = (1 - b)M_{\text{true}}$. SZ cluster masses calibrated on X-ray observations must also take this bias factor into account. When this bias factor is allowed to be large, the tension between CMB and SZ parameters is significantly reduced; the mass bias required to bring cluster observations into agreement with the CMB anisotropy is $b \approx 0.42$ (Planck Collaboration et al. 2016b). Adding a non-zero neutrino mass can also reduce the tension, but at the same time increases tension in other parameters predicted by *Planck* CMB and SZ. Notably, it lowers the *Planck* constraints for the Hubble constant (Planck Collaboration et al. 2016b). Though a number of explanations have been suggested to resolve this tension, the source of the disagreement is not yet agreed-upon within the community.

Dynamical cluster mass estimates provide a complementary way to explore the LSS-CMB tension. Dynamical mass estimates utilize the virial theorem, relating the LOS velocity dispersion of cluster members, σ_v , to cluster mass, M , as a power law. This approach famously led to Zwicky’s 1933 inference of dark matter in the Coma cluster. Hydrodynamical simulations find that the velocity dispersion of dark matter particles are similar to those of galaxies (e.g. Lau et al. 2010), though selecting only the brightest galaxies in a cluster tends to bias the galaxy velocity dispersion low (Saro et al. 2013; Wu et al. 2013). Because the dynamical mass method provides a relatively unbiased probe of cluster masses that is complementary to other cluster mass estimates, virial-theorem-based approaches are used in modern cluster mass estimates (e.g. Brodwin et al. 2010; Rines et al. 2010; Sifón et al. 2013; Ruel et al. 2014; Bocquet et al. 2015). Cluster counts as a function of velocity dispersion have also been proposed as a method for constraining cosmological parameters (Caldwell et al. 2016).

This work utilizes the Hectospec Survey of Sunyaev-Zeldovich-Selected Clusters (HECS-SZ, Rines et al. 2016). The HECS-SZ sample is an MMT/Hectospec spectroscopic follow up of a sample of 83 clusters selected from *Planck* observations. In their analysis of the HECS-SZ sample, Rines et al. (2016) find that these clusters are dynamically colder than expected, having smaller velocity dispersions, σ_v , than is predicted by a *Planck*-selected sample of clusters for the *Planck* fiducial cosmology. A mass bias together with a velocity bias of galaxies could explain the discrepancy. However, the biases required to remove the tension between CMB and cluster cosmological parameters would need to be large, in some cases, outside of the range presented

in recent literature. Rines et al. (2016) conclude that another explanation may be necessary to resolve the tension.

To explore the LSS-CMB tension, we utilize cluster line-of-sight velocity observations of the HECS-SZ sample in conjunction with a forward modeling dynamical approach. The cluster sample is analyzed using the Velocity Distribution Function (VDF), which was first introduced in Ntampaka et al. (2017). This method utilizes a forward-modeled test statistic that quantifies the abundance of clusters by measurements of their dynamics, through comparing summed probability density functions (PDFs) of clusters’ measured line-of-sight (LOS) velocities to that of a mock catalog.

We present a summary of the cluster observations, the mock observations, and the VDF methodology in Section 2, results and constraints on σ_8 and Ω_m in Section 3, and a discussion of the results in Section 4.

2. METHODS

2.1. HeCS-SZ

The Hectospec Survey of Sunyaev-Zeldovich-Selected Clusters (HECS-SZ, Rines et al. 2016) is an SZ-selected sample of clusters (Planck Collaboration et al. 2014c). The full *Planck*-selected sample contains 87 clusters selected above the 80% completeness limit of the *Planck* medium-deep sky or the 50% completeness limit of the *Planck* shallow sky (Planck Collaboration et al. 2014c); HECS-SZ comprises 83 clusters selected randomly from these 87 clusters. The sample ranges from redshift 0.05 up to 0.3 and utilizes SDSS DR6 Legacy and SDSS DR10 imaging as well as MMT/Hectospec spectroscopic follow up of potential cluster members. When two high-error galaxies are excluded, the remaining 25,112 galaxies in the HECS-SZ sample have mean line of sight velocity error of $\approx 30 \text{ km s}^{-1}$.

The cluster selection function of the HECS-SZ sample is shown in Figure 1. As redshift increases, so does the minimum mass a cluster must have to be detected by *Planck*; this is due to the *Planck* beam size. At high z and low M , the SZ signal is diluted by the large beam size, causing these clusters to have low signal to noise. The selection function is discontinuous at $z = 0.2$ because the HECS-SZ sample utilizes observations from two SDSS data releases. The sample for $z < 0.2$ utilizes observations from SDSS DR10 and has an effective sky area of 11589 deg^2 and a selection function that corresponds to *Planck*’s 80% completeness limit for the medium-deep sky. The sample for $0.2 < z < 0.3$ utilizes imaging observations from SDSS DR6 Legacy and spectroscopic observations from the Hectospec Cluster Survey (Rines et al. 2013). It has an effective sky area

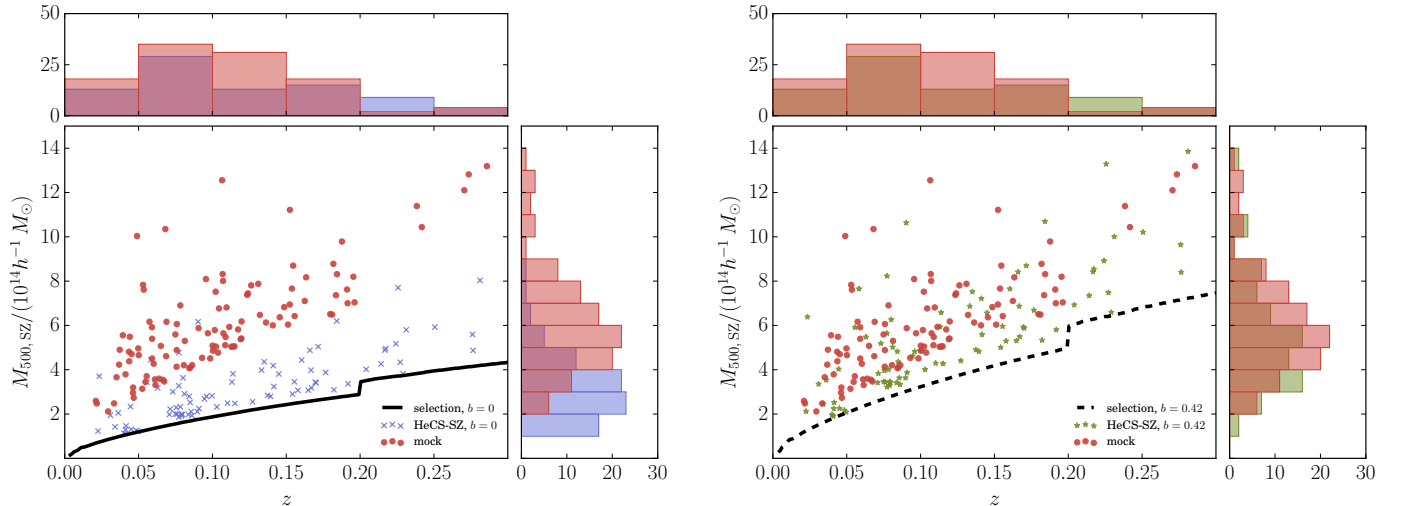


Figure 1. Left: The redshift and SZ mass ($M_{500,\text{SZ}}$) distribution of one sample mock observation (red circles) and that of the HECS-SZ sample with $b = 0$ (blue x's). The selection function with $b = 0$ (solid black curve) shows the limit above which the sample is modeled to have integral completeness $\mathcal{C} \in [0.6, 1.0]$, with $\mathcal{C} = 0.8$ shown. The discontinuity at $z = 0.2$ is due to two different observing methods being employed above and below this redshift. When the selection function is applied to the mock light cones, it is varied by a multiplicative factor of $(1 - b)^{-1}$ until the number of clusters above the selection function matches the number of clusters expected, given the HECS-SZ observation and choice of \mathcal{C} . The mock observation is clearly not in agreement with that of the HECS-SZ observation for $b = 0$. Right: [Planck Collaboration et al. \(2016b\)](#) reports a bias of $b = 0.42$ is needed to bring the *Planck* observed $M_{500,\text{SZ}}$ masses into agreement with the mass distributions predicted by the *Planck* CMB fiducial cosmology. When this bias is applied to the HECS-SZ observation (green stars) and selection function (black dash), the HECS-SZ sample is in better agreement with the mock observations, which assume the *Planck* fiducial cosmology. Summary PDFs of mass and redshift representative of the entire suite of mock observations are shown in Figure 2.

of 8417 deg^2 and the completeness limit jumps by 20% compared to the $z < 0.2$ sample.

Figure 1 shows the selection function of the HECS-SZ observation, as well as the redshift and SZ-determined M_{500} values of the 83 clusters in the HECS-SZ sample. The *Planck* medium-deep survey zone comprises 41.3% of the full sky, while the shallow survey zone comprises 56% (including the region around the Galactic Plane). Along the selection function shown in Figure 1, the likelihood of a cluster being detected by *Planck* is 80% for the medium-deep survey zone and 50% for the shallow survey zone. This likelihood increases with increased cluster SZ mass, $M_{500,\text{SZ}}$, therefore clusters lying above the selection function are more likely to be detected (See [Planck Collaboration et al. \(2014c\)](#) for complete details of the cluster selection function, survey zones, and completeness). To account for the varying completeness in this range, we define an integral completeness,

$$\mathcal{C} = \frac{N_{\text{observed}}}{N_{\text{true}}}, \quad (1)$$

the ratio of the number of *Planck*-detected clusters above the selection function to the true number of clusters in the sky and redshift regions of interest. We adopt a conservative flat prior of $\mathcal{C} \in [0.6, 1.0]$ on the integral completeness of the cluster sample.

The HECS-SZ M_{500} shown in this figure are calculated from the Y_{SZ} signal and reported by [Planck Collaboration et al. \(2014c\)](#). Figure 1 shows results for two sample values of the mass bias b , which parameterizes the scaling between a cluster's true mass and the observed M_{SZ} mass as $M_{\text{SZ}} = (1 - b)M_{\text{true}}$. A bias parameter of $b = 0.42$ is needed to bring SZ cluster masses into agreement with *Planck* CMB ([Planck Collaboration et al. 2014c](#); [Rines et al. 2016](#)), and employing this bias effectively increases the M_{500} values of the HECS-SZ clusters reported on the vertical axis of Figure 1. See [Rines et al. \(2016\)](#) for further details of the HECS-SZ observations.

A simple cylindrical cut is used to select apparent cluster members, including both true cluster members and interloping field galaxies, from the full HECS-SZ observation. This cylindrical cut uses angular extent and velocity cuts to correspond with the size and velocity dispersion of a cluster with $M_{200c} \geq 1 \times 10^{15} h^{-1} M_{\odot}$ at the *Planck* fiducial cosmology: a comoving $1.6h^{-1} \text{ Mpc}$ outer aperture, initial velocity cut of 2500 km s^{-1} about the cluster center and no σ_v velocity paring, according to the method detailed in [Ntampaka et al. \(2017\)](#).

The location of the cluster center in the plane of the sky and the location of the cluster velocity center are

both chosen iteratively. A cylinder with $R_{\text{aperture}} = 1.6h^{-1} \text{ Mpc}$ and $|v| \leq 2500 \text{ km s}^{-1}$ is centered initially on the SZ center and redshift of the cluster reported by [Planck Collaboration et al. \(2014c\)](#). The plane of sky center of mass and the mean velocity are calculated and the cylinder is recentered on this new location. The cylinder center iteratively moves in this manner until convergence (defined as $\Delta R < 0.02h^{-1} \text{ Mpc}$ and $\Delta v < 50 \text{ km s}^{-1}$); most clusters converge in one or two iterations.

The central region of the HECS-SZ observation is then removed; the resulting cylindrical selection has a $0.25h^{-1} \text{ Mpc}$ axial hole through the center. The velocity bias between substructure and dark matter particles is small in the outer regions of clusters but increases toward the center, making the outer region a better probe of the cluster’s dynamical state ([Aung et al., in prep.](#)). Furthermore, there may be systematic differences between the mock catalogs and HECS-SZ clusters due to the high concentration of galaxies in this region stemming from fiber collisions, observational selection effects, or distance resolution in the N -body simulation used to build the mock observation that destroys substructure near the center of simulated cluster.

Determining physical comoving distances to apply the fixed aperture requires some knowledge of the underlying cosmological parameters, and the measurement is particularly sensitive to Ω_m . We note that varying Ω_m by $\approx 10\%$ changes the effective aperture by $\lesssim 2\%$. Because this effect is relatively small, we opt to adopt the straightforward approach of assuming the *Planck* fiducial cosmology and a $1.6h^{-1} \text{ Mpc}$ comoving aperture for the HECS-SZ clusters.

2.2. Mock Observations

The mock observations are created from UniverseMachine ([Behroozi et al. 2018](#)) galaxies incorporated into the publicly available Multidark MDPL2 N -body simulation¹ ([Klypin et al. 2016](#)). The MDPL2 simulation uses a Λ CDM cosmology, with cosmological parameters consistent with the *Planck* CMB fiducial cosmology ([Planck Collaboration et al. 2014a](#)): $\Omega_\Lambda = 0.693$, $\Omega_m = 0.307$, $\Omega_b = 0.048$, $h = 0.678$, $n_s = 0.96$, and $\sigma_8 = 0.823$.

The MDPL2 simulation contains 3840^3 particles in a box with comoving length $1.0h^{-1} \text{ Gpc}$ with mass resolution of $1.51 \times 10^9 h^{-1} M_\odot$. Halo and subhalo properties are reported from the publicly available Rockstar halo catalog ([Behroozi et al. 2012](#)), and halo masses reported here are with respect to the critical density ρ_{crit} .

UniverseMachine is an empirical model of the merger history and star formation history of galaxies. The model paints galaxies onto halos and subhalos in the Multidark simulation using halo merger trees; halo mass, halo assembly history, and redshift all inform galaxy star formation rate. UniverseMachine tracks orphan galaxies, which are galaxies for which the hosting substructure has been numerically disrupted in the simulation, allowing for richer cluster mock observations than would be possible with the N -body simulation alone. All UniverseMachine galaxies with stellar mass $\geq 10^{9.5} h^{-1} M_\odot$ are used to construct the mock observations. Because the HECS-SZ sample has an average measurement error of $\approx 30 \text{ km s}^{-1}$, each galaxy in the mock catalog is given a velocity error selected from a Gaussian with width 30 km s^{-1} . For further details about the UniverseMachine galaxy catalog, see [Behroozi et al. \(2018\)](#) and references therein.

The UniverseMachine galaxies in comoving $1.0h^{-1} \text{ Gpc}$ snapshots for twelve redshifts ranging from $z = 0.0$ to $z = 0.304$ are used to construct eight full-sky light cones. The light cones differ only in the location at which the observer is placed. Each full-sky light cone is used to construct ten mock observations. These mock observations are modeled to follow the HECS-SZ observation closely: they adopt the redshift range ($0.05 < z < 0.3$) and sky area (11589 deg^2 for $z < 0.2$ and 8417 deg^2 for $0.2 < z < 0.3$) of HECS-SZ.

Y_{SZ} signals are assigned to each cluster with $M_{200} \geq 10^{14.2} h^{-1} M_\odot$ according to the power law relation from [Planck Collaboration et al. \(2016b\)](#), which assumes the universal pressure profile of [Arnaud et al. \(2010\)](#). The power law relation is employed with bias parameter $b = 0$ and lognormal scatter $\sigma_{\ln Y}$ included. The $Y_{\text{SZ}}(M_{\text{SZ}})$ relationship is inverted, and M_{SZ} values assigned to each cluster based on the cluster’s Y_{SZ} signal. Because this process includes scatter $\sigma_{\ln Y}$, it properly forward-models the sample of clusters which would be realistically observed and, therefore, accounts for Edington bias.

Apparent cluster members, including both true cluster members and interloping field galaxies, are selected with the same method described in Section 2.1: a simple cylindrical cut with a $1.6h^{-1} \text{ Mpc}$ aperture, initial velocity cut of 2500 km s^{-1} about the cluster center, and with no σ_v clipping. The cluster centers on the plane of the sky, as well as in velocity space, are determined by the same iterative scheme described in 2.1, and the central $0.25h^{-1} \text{ Mpc}$ is removed from the sample.

Figure 2 shows a PDF of mock catalog and HECS-SZ sample SZ masses and redshift. For $b = 0$, the distribution of masses disagrees significantly, but invoking a

¹ <http://www.cosmosim.org/>

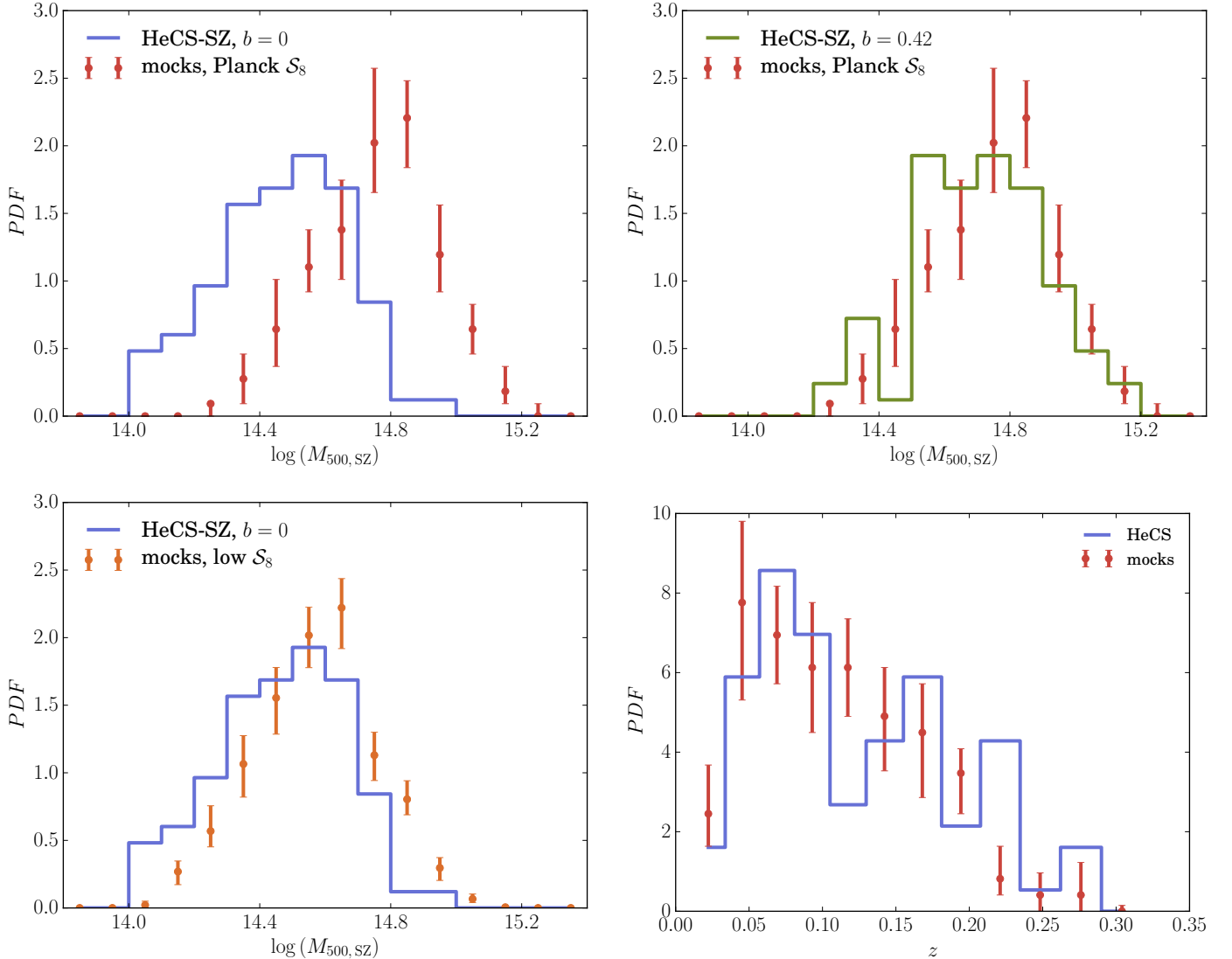


Figure 2. Top left: A PDF of cluster SZ masses, $M_{500,SZ}$ in units of $h^{-1} M_{\odot}$, assuming no mass bias. The HECS-SZ masses (blue solid) are as reported by *Planck*. Mock observation masses (red error bars showing the middle 68% of the mock observation PDF) include scatter in the $Y_{SZ}(M_{500,SZ})$ relationship to properly model Eddington bias. Top right: A significant bias must be applied to the HECS-SZ cluster masses ($b = 0.42$, green solid) to bring these into agreement with the masses predicted by the mock observations (red error bars) because the mock observations are built on a simulation that assumes the *Planck* CMB fiducial cosmology. Bottom left: Alternately, invoking a low \mathcal{S}_8 can bring the unbiased HECS-SZ observations (blue solid) into agreement with mock observations (orange error bars); $\mathcal{S}_8 = 0.70$ is shown for illustrative purposes. Bottom right: The range of redshift distributions in the fiducial cosmology mock observations (red error bars) and the HECS-SZ catalog (blue solid) have similar redshift distributions. For brevity, $\mathcal{C} = 0.8$ is shown.

mass bias of $b = 0.42$ can bring the mass distributions into agreement. Alternately, a mock catalog with a low value of \mathcal{S}_8 can also bring the mass distributions of the observed and simulated clusters into agreement. The redshift distribution of the HECS-SZ sample agrees with that of the mock catalog.

Mock observations for both the fiducial cosmology as well as for the nonfiducial cosmologies are calculated

as in [Ntampaka et al. \(2017\)](#). Briefly, each cluster is given a weight according to the cluster’s redshift, z , and mass, M_{200} , both of which are known quantities that are extracted from the simulation. This weight, w is given by

$$w = \frac{\text{HMF}(M, z, \sigma_8, \Omega_m)}{\text{HMF}(M, z, \sigma_{8,\text{sim}}, \Omega_{m,\text{sim}})} \quad (2)$$

the ratio of the nonfiducial analytic halo mass function (HMF) to the simulation HMF for the full $1.0h^{-1}$ Gpc box at the most appropriate redshift snapshot. For the analytic HMF we use that of [Tinker et al. \(2008\)](#) with an average halo density of $200\rho_{\text{crit}}$. Further details about the HMF of the Multidark suite of simulations can be found in [Comparat et al. \(2017\)](#).

The selection function shown in [Figure 1](#) is scaled by a multiplicative factor until the clusters above the selection have $\sum w = 87\mathcal{C}^{-1}$, where 87 is the number of clusters in the *Planck*-selected sample from which the 83 HECS-SZ clusters were randomly selected and \mathcal{C} is the integral completeness above the selection function.

The multiplicative scaling of the selection function of the mock observations relates to the bias factor that may be applied to the HECS-SZ observations, b , as $(1 - b)^{-1}$. Therefore, at the fiducial cosmology, a multiplicative scaling of 1.72 applied to the scaling relation shown in [Figure 1](#) is equivalent to the bias $b = 0.42$ that is needed to bring HECS-SZ cluster observations into agreement with the *Planck* CMB TT fiducial cosmology. [Figure 3](#) shows a histogram of biases needed to scale the simulation at the fiducial cosmology to match expected cluster counts for $\mathcal{C} = 0.8$. Biases that are slightly larger than the *Planck*-reported value are needed to bring the mock observations into full agreement with the observed cluster counts. This is due to the fact that the simulation uses the cosmological model at the central point of the *Planck* fiducial cosmology; simulations at lower

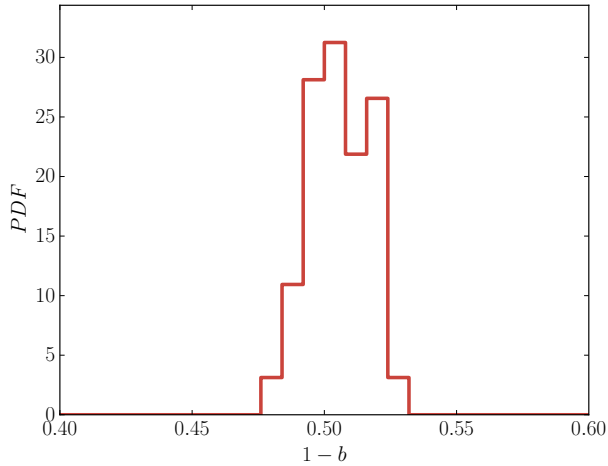


Figure 3. A PDF of bias, b , needed to scale the selection function (shown in [Figure 1](#)) to match the expected cluster counts for $\mathcal{C} = 0.8$. A significant bias is necessary to bring the observed cluster masses into agreement with that of a simulation at the *Planck* CMB fiducial cosmology. The PDF provides a way to explore this tension by utilizing cluster dynamical measurements.

\mathcal{S}_8 cosmologies, but still within the CMB TT constraint contours, would prefer lower biases.

In the case where cluster mass is defined by an average halo density with respect to the critical density, e.g. the $200\rho_{\text{crit}}$ definition used in this work, it is unlikely that the $M(\sigma_v)$ relation changes dramatically with changing Ω_m (e.g. [Evrard et al. 2008](#); [Okoli & Afshordi 2016](#)). Therefore, for nonfiducial, non-simulated cosmologies, cluster velocity distributions for individual clusters are assumed to remain unchanged.

2.3. Mock Observations with Systematics

In addition to the standard method outlined in [Section 2](#), we explore how systematic differences between the mock catalog and the HECS-SZ sample might affect the resulting \mathcal{S}_8 constraints. We construct eleven mock catalogs with systematics to explore this. The first four catalogs explore changes in parameters applied to both the HECS-SZ and mock catalog, while the remaining seven catalogs explore systematic changes to the mock catalogs only.

1. **Large Aperture:** To explore how the choice of cylinder size may bias the results, a large cylinder with $R_{\text{ap}} = 2.3h^{-1}$ Mpc, $v_{\text{cut}} = 3785\text{km s}^{-1}$, and $R_{\text{hole}} = 0.25h^{-1}$ Mpc is used to select galaxies in both the HECS-SZ sample and also in the mock catalog. The R_{ap} and v_{cut} values are selected to correspond to the typical radius and $2\sigma_v$ of a $3 \times 10^{15}h^{-1}M_{\odot}$ cluster.
2. **No Axial Hole:** To explore how the choice of axial hole may bias the constraints, no axial hole is removed from the cylinder center. All other parameters of the standard catalog remain unchanged. This change is applied to both the HECS-SZ sample and also to the mock catalog.
3. **Sigma Clipping:** To reduce the effects of interlopers, 2-sigma iterative velocity clipping is applied both to the HECS-SZ sample and also to the mock catalogs. Additional details about this iterative clipping can be found in [Ntampaka et al. \(2017\)](#).
4. **Low Redshift:** To explore whether the constraints are driven by the high-mass sample at high redshift, these clusters are removed from the sample. Both the HECS-SZ sample and also the mock catalogs are limited to samples with $z \leq 0.2$.
5. **Y-M Scatter:** To explore whether an underestimation of the scatter in the Y-M scaling relation may bias the results, the level of scatter in the

Y-M scaling relation is increased by 50%. This change is applied only to the mock catalog to assess for a potential systematic difference between the mock and HECS-SZ samples. The increase in scatter effectively makes the average mass of the mock sample smaller by scattering low-mass clusters above the selection function shown in Figure 1.

6. **Radial Selection:** To explore whether small differences between the HECS-SZ sample and the mock observation in the radial distribution function (RDF, discussed in detail in Section 2.5) bias the results, the mock clusters are subsampled to match the HECS-SZ RDF.
7. **Rich Clusters:** To explore how the choice of richness may bias the constraints, only rich clusters, defined as having at least 40 galaxies, are included in the mock catalog.
8. **Reduced Interlopers:** To explore whether an overabundance of interlopers may bias the results, the threshold mass for interlopers is increased to $M_{200} \geq 10^{12} h^{-1} M_{\odot}$. This change is applied only to the mock catalog to assess for a potential systematic difference between the mock and HECS-SZ samples. The increase in interloper mass cut effectively decreases the number of interloping galaxies in the mock catalog.
9. **Red Fraction:** HECS-SZ galaxies are preferentially selected to lie on the red sequence and therefore are more likely to be cluster members (and less likely to be interlopers) than a stellar-mass-selected sample. To test for a bias from preselecting likely cluster members, we select galaxies from the mock catalog with a similar bias towards cluster members. This is done by subsampling true cluster members to 80% of the original galaxy population and interloping field galaxies to 20% of the original galaxy population. This change is applied to the mock sample only.
10. **Quiescent Galaxies:** HECS-SZ galaxies are preferentially selected to lie on the red sequence, while the sample in the standard catalog is mass-selected. Differences are found between the velocity dispersions of red galaxies versus the velocity dispersions of all galaxies in a cluster sample, with velocity dispersions of a color-selected sample mildly biased compared to that of a stellar-mass-selected sample (e.g. Biviano et al. 2002; Goto 2005; Biviano et al. 2006; Gifford et al. 2013;

Owers et al. 2017; Farahi et al. 2018; Bilton & Pimblet 2018). To test for a bias stemming from differences in galaxy selection, we select galaxies from the mock catalog with specific star formation rate (sSFR) $\leq 10^{-2} \text{ Gyr}^{-1}$ (as in, e.g., Schaye et al. 2015). This change is applied to the mock sample only.

11. **Biased Velocities:** To further explore how velocity bias may affect the resulting constraints, we artificially impose a velocity bias on the galaxies in the standard mock catalog, reducing the velocity of every galaxy in the mock catalog to 0.95 times its true value. It should be noted that this check likely overemphasizes the true velocity bias in two ways: first, by imposing the bias on all galaxies in the sample, including interlopers, and second, by failing to disentangle the fact that this bias tends toward zero for well-sampled clusters (Saro et al. 2013). This change is applied to the mock sample only.

Unless otherwise noted, all parameters are identical to the standard catalog and the method is applied to both the HECS-SZ sample as well as to the mock catalog. Table 1 summarizes the key details of these mock catalogs with systematics.

2.4. The Velocity Distribution Function

The velocity distribution function (VDF, Ntampaka et al. 2017) is a forward-modeled test statistic that can be used to compare distributions of observed cluster member velocities to those predicted with simulations. The VDF can be used directly to explore constraints on cosmological parameters and is less affected by measurement errors associated with dynamical masses or the resulting Eddington bias (Eddington 1913). The VDF, $dn(v)/dv$, is the sum of probability distribution functions (PDFs) of galaxy LOS velocities and is given by

$$\frac{dn}{dv}(v) = \left[\frac{1}{N} \sum_{i=1}^N [\text{PDF}(|v|)]_i \right]_{A, z_{\min}, z_{\max}}, \quad (3)$$

where $\text{PDF}(|v|)$ denotes a probability distribution function of the absolute value of galaxy LOS velocities, the index i denotes a sum over N clusters (83 for the HECS-SZ sample and $87 \times \mathcal{C}^{-1}$ for the mock observations), A indicates that the VDF is calculated for a given sky area, and z_{\min}, z_{\max} indicates that the VDF is calculated for a

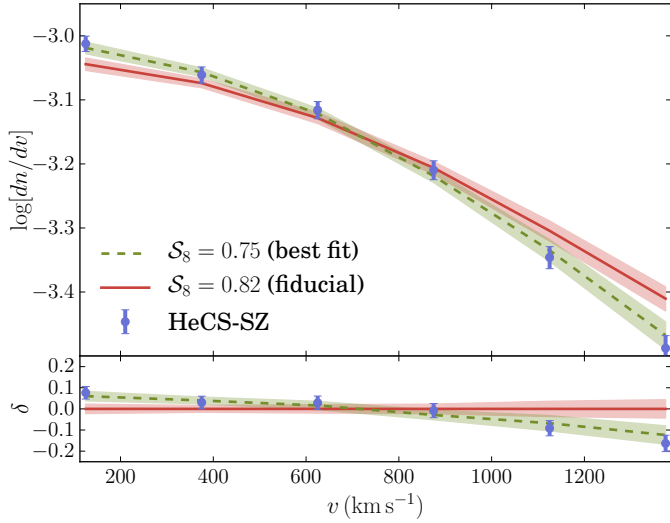


Figure 4. Top panel: The VDF of the mock observations at two different cosmologies (colored curves with band indicating the middle 68% of mock observations), for the standard catalog with integral completeness $\mathcal{C} = 0.8$. There is a dearth of high-velocity members in the HECS-SZ catalog (blue points with Poisson error bars) compared to the fiducial cosmology ($\mathcal{S}_8 = 0.82$, red solid), but a lower \mathcal{S}_8 cosmology (e.g. $\mathcal{S}_8 = 0.75$, green dash) is more consistent with the data. This agrees with the results of the top left panel of Figure 2, which shows that unless one invokes a significant mass bias, there are fewer high-mass clusters in the HECS-SZ observation than in the mock observations. Bottom panel: The fractional difference between models, δ , is the largest at very high and very low velocities, where the technique has the most resolving power. Near $\approx 800 \text{ km s}^{-1}$, δ crosses 0, indicating that bins near these central velocities are not as useful in differentiating models.

given redshift range². We use six velocity bins of width $\Delta v = 250 \text{ km s}^{-1}$, with edges from 0 to 1500 km s^{-1} .

The resulting VDF is shown in Figure 4. As in Ntampaka et al. (2017), the VDF has the most resolving power at high and low velocities. The crossover point where velocity bins have no resolving power has shifted downward from $\approx 1200 \text{ km s}^{-1}$ in Ntampaka et al. (2017) to $\approx 800 \text{ km s}^{-1}$; this is due to the changes in the cluster selection method and effective volume compared to the previous tests on mock catalogs.

The VDF in Figure 4 shows that the HECS-SZ clusters are dynamically colder than those in the simulation

at the fiducial cosmology, since the VDF has a dearth of high-velocity members compared to the mock observation at the fiducial cosmology. As was noted in Rines et al. (2016), the HECS-SZ clusters have a smaller σ_v than expected from a *Planck*-selected cluster sample at the *Planck* CMB fiducial cosmology. This could be caused by a number of factors, including a true dearth of high-mass clusters or a bias between velocity dispersions in the simulations and those of observed clusters.

Figure 5 shows the VDF for mock catalogs with systematics, which explore how parameter choices or possible biases between the HECS-SZ sample and mock observations may introduce bias to the results. For complete details on the parameter choices for each of the mock catalogs with systematics, see Section 2.3.

Four of the mock catalogs with systematics (Large Aperture, No Axial Hole, Sigma Clipping, and Low Redshift) assess parameter choices. For these catalogs, we change one of the standard parameter choices, and apply this change to both the mock catalog as well as the HECS-SZ sample. As can be seen in Figure 5, both the mock catalog VDF as well as the HECS-SZ VDF change compared to the standard version in Figure 4. This change is most pronounced in the sigma clipping example, with a decrease in signal at the high velocity end of the VDF. In all cases, the HECS-SZ VDF signal lies below (above) the fiducial mock VDF signal at high (low) velocities, and is in much closer agreement with a low \mathcal{S}_8 cosmology.

The remaining seven mock catalogs with systematics (Y-M Scatter, Radial Selection, Rich Clusters, Reduced Interlopers, Red Fraction, Quiescent Galaxies, and Biased Velocities) involve changes to the mock VDF only; the HECS-SZ VDF signal is the same as is shown for the standard catalog in Figure 4. The changes impart small changes on the mock VDF, but none of these changes are sufficient to pull the HECS-SZ sample into agreement with the $\mathcal{S}_8 = 0.82$ fiducial cosmology VDF. (There is one exception, the Biased Velocities catalog, which is within 1σ of $\mathcal{S}_8 = 0.82$, but as discussed previously, this catalog likely overestimates a realistic velocity bias, with the Quiescent Galaxies catalog being a more proper modeling of this effect.) The result is robust to these explorations of possible systematics: the HECS-SZ clusters are dynamically colder than those in the simulation at the fiducial cosmology.

² Note that the VDF takes a slightly different form than the one presented in Ntampaka et al. (2017). Here, we have removed the volume element, which is sensitive to the underlying cosmological parameters, and instead defined the test statistic by limits on parameters that are invariant under changes in cosmology: sky area, redshift range, and the number of clusters observed.

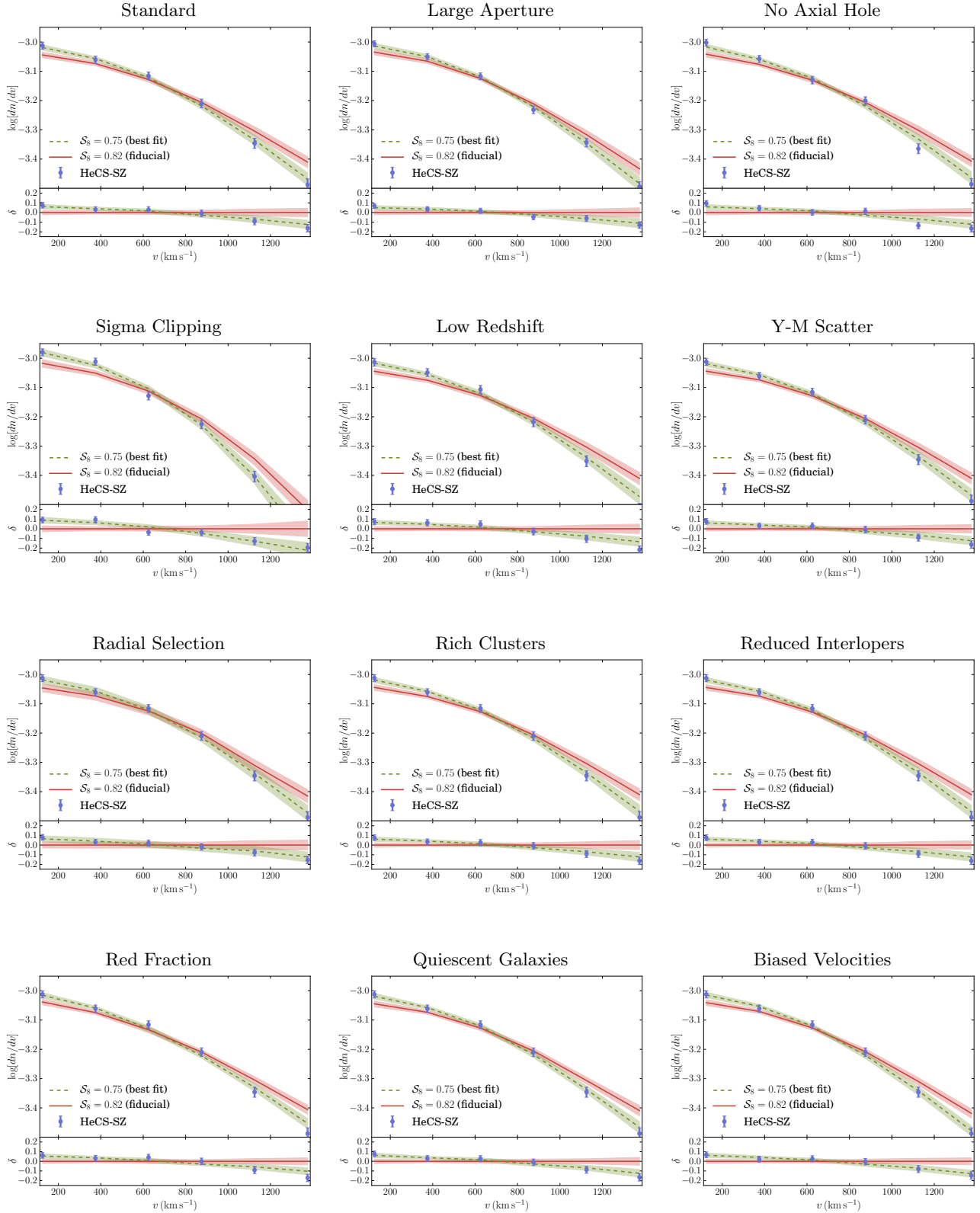


Figure 5. The VDF, plotted in the same format as in Figure 4, for the mock catalogs with systematics. The catalogs are described in detail in Section 2.3 and serve to explore how parameter choices and possible systematic differences between the HeCS-SZ sample and mock catalogs may affect the resulting constraints. These have remarkably small effects: the HeCS-SZ catalog (blue points with error bars) has fewer high-velocity galaxies compared to the fiducial mock catalog (red) and is in much better agreement with a lower- S_8 cosmology (shown is the standard catalog best fit catalog, green) for all of the alternative catalogs.

2.5. Radial Distribution Function

The radial distribution function (RDF) is used as a self-consistency check to evaluate the relative radial distributions of galaxies. It is calculated as a sum of comoving radial distance PDFs and is given by

$$\frac{dn}{dR_{\text{sep}}}(R_{\text{sep}}) = \left[\frac{1}{N} \sum_{i=1}^N [\text{PDF}(R_{\text{sep}})]_i \right]_{A, z_{\text{min}}, z_{\text{max}}}, \quad (4)$$

where R_{sep} is the projected radial distance from the galaxy to the cluster center, $\text{PDF}(R_{\text{sep}})$ denotes a probability distribution function of the projected comoving distance from the cluster center under the assumption of the fiducial cosmology, the index i denotes a sum over N clusters, and $A, z_{\text{min}}, z_{\text{max}}$ indicates that the RDF is calculated for a given sky area and redshift.

Figure 6 shows the RDF for the mock clusters, which are based on the fiducial cosmology, and the HECS-SZ clusters. The error bars on the HECS-SZ RDF is created by allowing Ω_m and h to vary within an ellipse defined by the TT+lowP $2\text{-}\sigma$ constraints reported by Planck Collaboration et al. (2016a): Ω_m varies from 0.29 to 0.34 and h varies from 0.65 to 0.69. The error band on the RDF of the mock observations shows the middle 68% and 95% of the individual mock observation RDFs at the fiducial cosmology.

When evaluated at the fiducial cosmology, the HECS-SZ RDF is somewhat more centrally peaked than the mock observations, though the difference is subtle. One explanation for this is that the HECS-SZ sample may contain fewer massive clusters. Alternately, galaxy selection effects, cluster selection effects, or baryonic effects may be the source of the disagreement, which is not fully explained by allowing Ω_m and h to vary to extreme values. The effect of galaxy selection is explored by subsampling the mock catalog to match the HECS-SZ sample RDF in the Radial Selection catalog described in Section 3 and Table 1.

3. RESULTS

3.1. Credible Regions

The posterior probability, $P(\sigma_8, \Omega_m | y)$, of a model given the HECS-SZ observation is calculated as in Ntampaka et al. (2017). Briefly, the estimated covariance matrix, \hat{C} , is given by

$$\hat{C} = \frac{1}{n_{\text{mock}} - 1} \sum_{i=1}^{n_{\text{mock}}} [(y_i - \bar{y})(y_i - \bar{y})^T], \quad (5)$$

where i denotes a sum over the $n_{\text{mock}} = 80$ fiducial mock observations, n_{bin} is the number of velocity bins, y_i is a $n_{\text{bin}} \times 1$ column vector of the i^{th} mock observation's

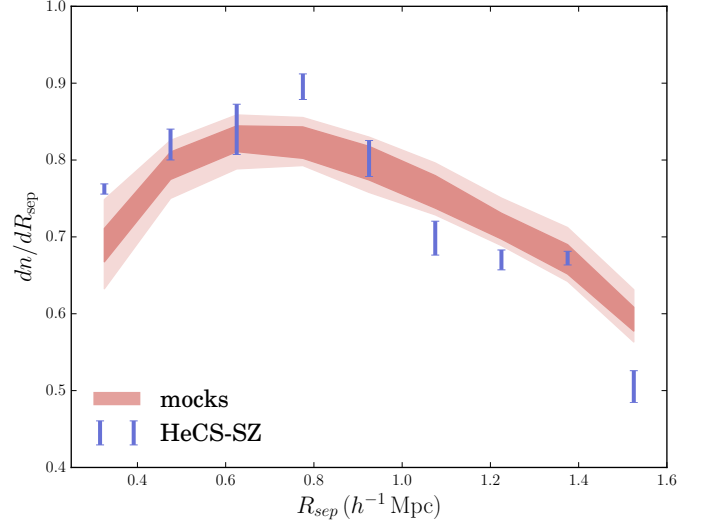


Figure 6. The radial distribution function (RDF) of the mock observations and HECS-SZ clusters. Parameters Ω_m and h affect the inferred R_{sep} , and allowing these parameters to vary within the $2\text{-}\sigma$ values reported by Planck Collaboration et al. (2016a) produces a band of RDF curves for the mock observations (dark and light red bands showing the middle 68% and 95%, respectively). The RDF of the HECS-SZ sample (blue with Poisson error bars) is subtly more centrally peaked than the RDF of the mock observation. Sub-sampling the mock observation to match the HECS-SZ RDF to account for possible galaxy selection effects is explored in the Radial Selection catalog (see Sections 2.3 and Table 1). Alternately, the difference may be due to the HECS-SZ sample containing less massive clusters with a smaller physical extent than the mock observation clusters.

n_{bin} bin values, and \bar{y} is a $n_{\text{bin}} \times 1$ column vector of the HECS-SZ observation.

As detailed in, e.g., Hartlap et al. (2007); Taylor et al. (2013); Percival et al. (2014), an unbiased estimator, $\hat{\Psi}^{-1}$, of the inverse covariance matrix is given by

$$\hat{\Psi}^{-1} = \frac{n_{\text{mock}} - n_{\text{bin}} - 2}{n_{\text{mock}} - 1} \hat{C}^{-1}, \quad (6)$$

where \hat{C}^{-1} denotes a standard matrix inversion of the covariance matrix. The χ^2 values are calculated by

$$\chi^2(y | \sigma_8, \Omega_m) = (\bar{y} - y^*)^T \hat{\Psi}^{-1} (\bar{y} - y^*), \quad (7)$$

where y^* is a $n_{\text{bin}} \times 1$ column vector of average mock observation VDF signal at a single cosmology and \bar{y} is the measured HECS-SZ VDF signal. The unbiased estimator of the inverse covariance matrix, $\hat{\Psi}^{-1}$, is calculated at the fiducial cosmology and assumed to be constant across the $\sigma_8\text{-}\Omega_m$ plane. This assumption breaks down as models farther from the fiducial model are considered. To properly analyze the VDF and the constraints

in the σ_8 - Ω_m plane, one would need a suite of simulations across multiple σ_8 and Ω_m models.

We find that, for a given integral completeness \mathcal{C} , the likelihood $\mathcal{L}(\mathcal{S}_8|\mathcal{C})$ is well modeled by a Gaussian in \mathcal{S}_8 with constant variance σ^2 and mean $\mu(\mathcal{C})$ that varies linearly with integral completeness, $\mathcal{C} \equiv N_{\text{observed}}/N_{\text{true}}$.

To account for uncertainties in integral completeness, which was not an unknown quantity in [Ntampaka et al. \(2017\)](#), we add an additional step to the statistical inference by including priors on \mathcal{S}_8 and \mathcal{C} . The posterior π takes the form

$$\pi(\mathcal{S}_8 | \bar{y}, \mathcal{C}, \sigma) \propto \mathcal{L}(\mathcal{S}_8 | \mathcal{C}, \sigma) \pi_1(\mathcal{S}_8) \pi_2(\mathcal{C}) \quad (8)$$

where the likelihood is a Gaussian

$$\mathcal{L}(\mathcal{S}_8 | \mathcal{C}, \sigma) \propto \exp\left(-\frac{[\mathcal{S}_8 - \mu(\mathcal{C})]^2}{(2\sigma)^2}\right), \quad (9)$$

$\pi_1(\mathcal{S}_8)$ is a flat prior on \mathcal{S}_8 , $\mathcal{S}_8 \in [0.0, 1.0]$, and $\pi_2(\mathcal{C})$ is a flat prior on completeness, $\mathcal{C} \in [0.6, 1.0]$.

The credible regions are calculated between $\Omega_m = 0.28$ and $\Omega_m = 0.33$; this function takes the form

$$\mathcal{S}_8 = \sigma_8 \left(\frac{\Omega_m}{0.3}\right)^\gamma \quad (10)$$

where the power law parameter γ describes the direction of the degeneracy in the σ_8 - Ω_m plane and the parameter \mathcal{S}_8 can be interpreted as the preferred value of σ_8 at $\Omega_m = 0.3$.

Figure 7 shows the 68% and 95% credible regions. We find constraints in the σ_8 - Ω_m plane given by $\sigma_8 (\Omega_m/0.3)^{0.25} = 0.751 \pm 0.037$, as shown in Figure 7. The *Planck* CMB TT fiducial cosmology lies outside of our 95% credible region, but constraints from *Planck* SZ cluster counts ([Planck Collaboration et al. 2014a](#)), the KiDS+VIKING-450 cosmic shear analysis ([Hildebrandt et al. 2018](#)) and DES Year 1 Results for Λ CDM ([DES Collaboration et al. 2017](#)) lie within 1σ of our reported constraints. More recent *Planck* cluster count results invoking mass bias (baseline results, [Planck Collaboration et al. 2016b](#)), Weighing the Giants ([Mantz et al. 2015](#)), and South Pole Telescope ([de Haan et al. 2016](#)) have maximum likelihood functions that are within 2σ of our reported constraints near $\Omega_m = 0.3$.

Note that while some other definitions of \mathcal{S}_8 use a γ parameter of either $\gamma = 0.5$ (e.g. [Hildebrandt et al. 2017](#)) or $\gamma = 0.3$ (e.g. [Planck Collaboration et al. 2014b](#)). We allow γ to be informed by the data rather than adopting a more standard definition, but for values of Ω_m near the Ω_m normalization value of 0.3, these disparate definitions of \mathcal{S}_8 can be compared. It is only far from the Ω_m normalization value of 0.3 that the degeneracy direction γ separates these different definitions of \mathcal{S}_8 .

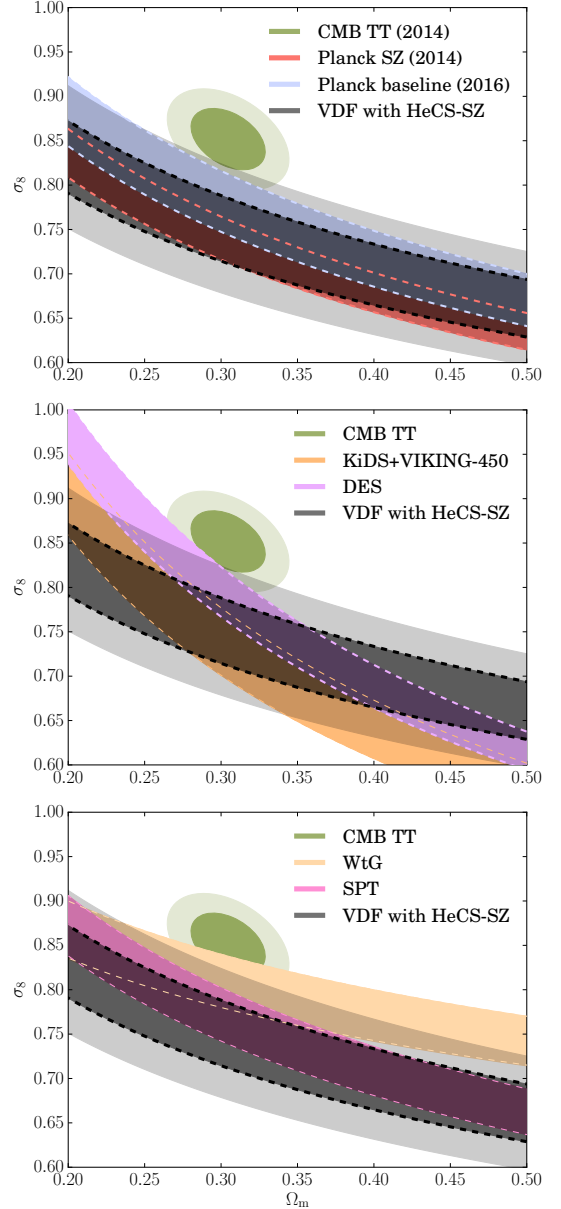


Figure 7. VDF cosmological constraints on σ_8 and Ω_m (black, 68% and 95% contours, all plots). The *Planck* CMB TT fiducial cosmology (green, 1- and 2- σ contours, all plots) prefers a high σ_8 . [Planck Collaboration et al. \(2014a\)](#) constraints from *Planck* SZ cluster counts (red, top plot) prefers a low σ_8 if mass bias is not invoked, while more recent cluster-based results invoking mass bias from [Planck Collaboration et al. \(2016b\)](#) CCCP + BAO + BBN [Baseline] (blue, top plot) lie below, though not in tension with, the *Planck* CMB fiducial cosmology. The KiDS+VIKING-450 cosmic shear analysis (orange, center plot, [Hildebrandt et al. 2018](#)) also lies below the *Planck* CMB fiducial cosmology. [DES Collaboration et al. \(2017\)](#) Year 1 Results for Λ CDM (purple, middle plot), Weighing the Giants (peach, bottom plot, [Mantz et al. 2015](#)), and South Pole Telescope (pink, bottom plot, [de Haan et al. 2016](#)) lie below, though not in tension with, the *Planck* fiducial cosmology.

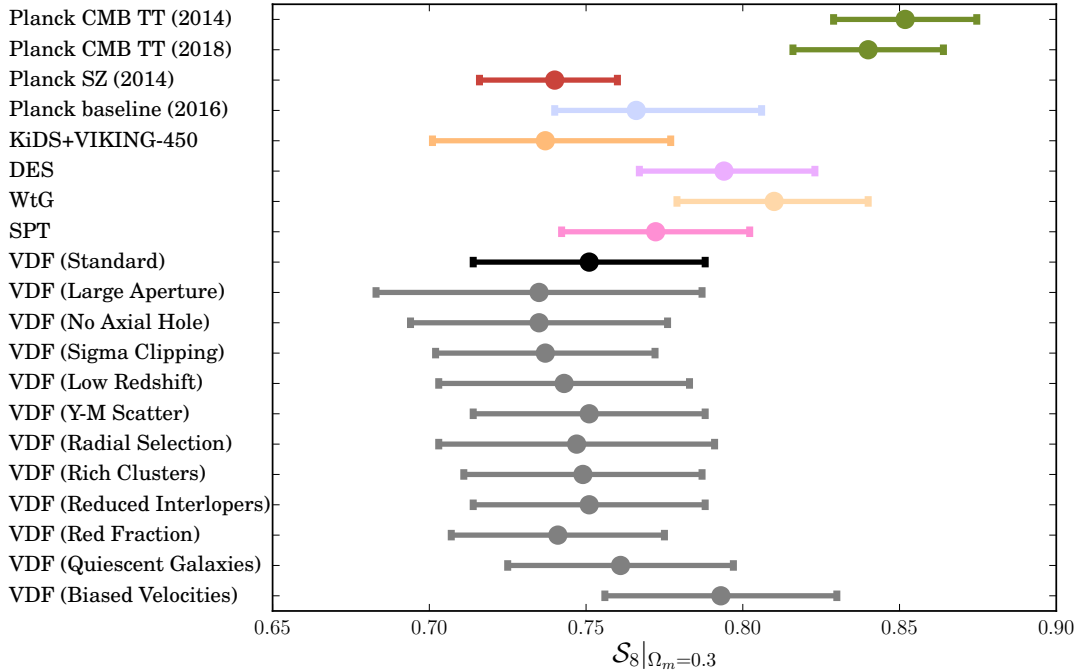


Figure 8. \mathcal{S}_8 constraints evaluated at $\Omega_m = 0.3$ for a variety of cosmological probes. *Planck* CMB TT (2014), SZ, and baseline, as well as KiDS+VIKING-450 cosmic shear, DES, WtG, SPT, and VDF (Standard) are the same as are shown in Figure 7. More recent *Planck* CMB TT results (Planck Collaboration et al. 2018) are also shown in green. The Biased Velocities catalog (discussed in detail in Sections 2.3 and 1) artificially imposes a fractional velocity bias on all galaxies in the mock catalog, likely overestimating the true velocity bias, and may overestimate \mathcal{S}_8 constraints as a result. Constraints from the remaining catalogs with systematics show remarkable agreement, with central values within $\frac{1}{2}\sigma$ of the standard catalog.

3.2. \mathcal{S}_8 Constraints for Mock Catalogs with Systematics

Figure 8 shows a summary of \mathcal{S}_8 constraints evaluated at $\Omega_m = 0.3$. This figure shows the sample of recent probes of \mathcal{S}_8 that were highlighted in Figure 7, constraints of \mathcal{S}_8 from the VDF standard catalog, and also constraints of \mathcal{S}_8 for the mock catalogs with systematics. Our constraints on \mathcal{S}_8 are remarkably robust to the changes in catalog parameters that are explored by the eleven additional mock catalogs.

The Biased Velocities and Quiescent Galaxies catalogs constraints prefer the largest \mathcal{S}_8 . The Biased Velocities catalog (0.793 ± 0.037 , with a center that is $\approx 1.15\sigma$ from the standard catalog), as discussed in Section 2.3, overemphasizes the true velocity bias in two ways: first, by imposing the bias on all galaxies in the sample, including interlopers, and second, by failing to disentangle the fact that this bias tends toward zero for well-sampled clusters (Saro et al. 2013). Supporting the relevance of the second of these caveats, four clusters from the HECS-SZ sample are studied in detail in Rines et al. (2013), with the authors finding no significant bias in the estimates of velocity dispersions of red-sequence galaxies compared to the full galaxy sample. Though the value

of 0.95 may be an overestimate of the bias found in the HECS-SZ cluster sample, it nonetheless provides an important cross-check for understanding how velocity bias might affect the resulting cosmological constraints.

In the case of the Quiescent Velocities catalog ($\mathcal{S}_8 = 0.761 \pm 0.036$), in selecting only the quiescent galaxies in the mock catalog, the number of high-velocity galaxies is somewhat reduced. This results in constraints preferring a slightly larger \mathcal{S}_8 , though still within $\frac{1}{2}\sigma$ of the standard method. This can be understood in the context of velocity segregation (Biviano et al. 2002; Owers et al. 2017; Farahi et al. 2018), with red or quiescent galaxies having a velocity dispersion that may be $\approx 5\%$ smaller than that of the full cluster sample (Goto 2005; Biviano et al. 2006; Gifford et al. 2013; Bilton & Pimblett 2018), and can be attributed to the fact that blue galaxies are typically infalling and, therefore, have higher velocities. However, it should be noted that the effect becomes smaller with well-sampled clusters (Saro et al. 2013) and recent simulations find a stellar-mass-selected sample to be relatively unbiased ($< 5\%$ in Armitage et al. (2018)), and both of these may contribute to the fact that the Quiescent Velocities constraints are not as extreme as the Biased Velocities constraints.

Table 1. Catalog Summary

Approach	Description	Parameter Constraints
Standard	$R_{\text{ap}} = 1.6h^{-1} \text{ Mpc}$, $v_{\text{cut}} = 2500 \text{ km s}^{-1}$, $R_{\text{hole}} = 0.25h^{-1} \text{ Mpc}$, $N_{\text{min}} = 20$	$\mathcal{S}_8 = \sigma_8 (\Omega_m/0.3)^{0.25} = 0.751 \pm 0.037$
Large Aperture	$R_{\text{ap}} = 2.3h^{-1} \text{ Mpc}$, $v_{\text{cut}} = 3785 \text{ km s}^{-1}$	$\mathcal{S}_8 = \sigma_8 (\Omega_m/0.3)^{0.25} = 0.735 \pm 0.052$
No Axial Hole	$R_{\text{hole}} = 0.0h^{-1} \text{ Mpc}$	$\mathcal{S}_8 = \sigma_8 (\Omega_m/0.3)^{0.25} = 0.735 \pm 0.041$
Sigma Clipping	$\sigma_{\text{clip}} = 2.0$	$\mathcal{S}_8 = \sigma_8 (\Omega_m/0.3)^{0.25} = 0.731 \pm 0.035$
Low Redshift	Limit catalogs to clusters with $z \leq 0.2$.	$\mathcal{S}_8 = \sigma_8 (\Omega_m/0.3)^{0.25} = 0.743 \pm 0.040$
Y-M Scatter	50% additional scatter in Y-M relation.	$\mathcal{S}_8 = \sigma_8 (\Omega_m/0.3)^{0.25} = 0.751 \pm 0.037$
Radial Selection	Force simulation RDF to match observed RDF by downsampling mock observation.	$\mathcal{S}_8 = \sigma_8 (\Omega_m/0.3)^{0.25} = 0.747 \pm 0.044$
Rich Clusters	$N_{\text{min}} = 40$	$\mathcal{S}_8 = \sigma_8 (\Omega_m/0.3)^{0.25} = 0.749 \pm 0.038$
Reduced Interlopers	Higher threshold for interlopers; interlopers must live in a halo with $M_{200} \geq 10^{12}h^{-1} M_{\odot}$.	$\mathcal{S}_8 = \sigma_8 (\Omega_m/0.3)^{0.25} = 0.751 \pm 0.037$
Red Fraction	Randomly select 80% of true members and 20% of interlopers to form the mock observation.	$\mathcal{S}_8 = \sigma_8 (\Omega_m/0.3)^{0.25} = 0.741 \pm 0.034$
Quiescent Galaxies	Select only galaxies with $\text{sSFR} \leq 10^{-1} \text{ Gyr}^{-1}$.	$\mathcal{S}_8 = \sigma_8 (\Omega_m/0.3)^{0.25} = 0.761 \pm 0.036$
Biased Velocities	Artificially bias the velocities of all mock galaxies.	$\mathcal{S}_8 = \sigma_8 (\Omega_m/0.3)^{0.25} = 0.793 \pm 0.037$

Table 1 briefly describes the mock catalogs with systematics and also gives the parameter constraints on \mathcal{S}_8 for each. Regardless of the choice of parameters, each approach yields a preference for a low \mathcal{S}_8 and all catalogs (except for the Biased Velocities catalog) have a central value within $\frac{1}{2}\sigma$ of the standard method. While properly assessing the systematic error due to the choice of modeling parameters would require more thoroughly sampling the high-dimensional space of these parameters, this result suggests that the systematic error is of the order one-half the statistical error.

4. DISCUSSION & CONCLUSION

The abundance of clusters as a function of mass and redshift is a valuable tool for constraining cosmological models. Notably, the cosmological parameters based on *Planck* CMB observations predict more high-mass clusters than are observed. Biases in cluster mass estimates remain at the forefront of the discussion in interpreting cluster mass observations and resolving the tension between *Planck* CMB cosmological parameters and cluster counts.

Eddington bias, caused by the steeply declining mass function coupled with errors in mass estimates, produces an observed halo mass function with an upscatter of high-mass clusters. Accounting for this bias must be done correctly, and assumptions about the distribution of scatter handled carefully. The velocity distribution function (VDF) is a forward-modeled test statistic that can be used to quantify the abundance of galaxy clusters in a way that is less sensitive to biases introduced by measurement error than more standard HMF approach.

We have used the VDF to compare the summed velocity PDFs of observed HECS-SZ clusters to mock observations produced by N -body simulations. In agreement with Rines et al. (2016), we find that this collection of clusters are dynamically colder than expected, having smaller velocities than one would predict for a *Planck*-selected sample of clusters for the *Planck* fiducial cosmology. This suggests that the observed clusters may be less massive than an $\mathcal{S}_8 = 0.82$ cosmology would predict. We have explored several possible sources of systematic error, including parameter choices, interloper fraction, velocity bias, and galaxy selection effects. Our results are remarkably robust to reason-

able changes to the standard mock catalog. While the precise fit of our preliminary constraints has a small dependence on the details of the model, all approaches show a preference for a low \mathcal{S}_8 , and our standard approach gives credible regions in the σ_8 - Ω_m plane given by $\mathcal{S}_8 \equiv \sigma_8 (\Omega_m/0.3)^{0.25} = 0.751 \pm 0.037$.

The constraints presented here should not be overinterpreted. The missing high-velocity members may be caused by a true dearth of high-mass clusters, or may alternately be caused by a bias between simulated cluster substructure velocity and cluster member velocities. Also, assumptions of a smoothly-varying covariance matrix break down far from the fiducial model. Similarly, the fraction and characteristics of interlopers are a function of cosmological parameters; these will also change far from the simulated fiducial cosmology. Properly evaluating the covariance matrices and interloper population of non-fiducial (or non-simulated) cosmologies would require a suite of large volume, high resolution simulations to capture the nuanced correlations. Furthermore, properly evaluating these with realistic galaxy selection effects may require a large suite of hydrodynamical simulations that properly model galaxy properties. Such a suite of simulations could also eliminate the need to assume cosmological parameters in the calculation of comoving distances, which could instead be replaced with invariant parameters such as angular extent.

Other LSS and cluster-based analyses have found similar results, seeing a tension between observations and the *Planck* CMB cosmology, and preferring smaller \mathcal{S}_8

values (or needing to invoke new physical models) to explain the discrepancy (e.g. Heymans et al. 2013; Hildebrandt et al. 2017; Leauthaud et al. 2017; Lin & Ishak 2017). The VDF provides a complementary test to use clusters as a cosmological probe. As observations probe larger areas of the sky to deeper magnitudes become available, these data sets will provide opportunities to understand and resolve the tension in \mathcal{S}_8 constraints.

We thank our anonymous referee for their helpful feedback on this manuscript. We also thank Peter Behroozi, Risa Wechsler, Andrew Hearin, and Charlie Conroy for early access to the UniverseMachine Catalog as well as Sownak Bose, Jessi Cisewski-Kehe, Daniel Eisenstein, Gus Evrard, Arthur Kosowsky, Rachel Mandelbaum, Frank van den Bosch, and Alexey Vikhlinin for their valuable feedback on this project. Hy Trac is supported in part by DOE grant DE-SC0011114 and NSF grant IIS-1563887. The CosmoSim database used in this paper is a service by the Leibniz-Institute for Astrophysics Potsdam (AIP). The MultiDark database was developed in cooperation with the Spanish MultiDark Consolider Project CSD2009-00064. The Bolshoi and MultiDark simulations have been performed within the Bolshoi project of the University of California High-Performance AstroComputing Center (UC-HiPACC) and were run at the NASA Ames Research Center. The MultiDark-Planck (MDPL) and the BigMD simulation suite have been performed in the Supermuc supercomputer at LRZ using time granted by PRACE.

REFERENCES

- Armitage, T. J., Barnes, D. J., Kay, S. T., et al. 2018, MNRAS, 474, 3746
- Arnaud, M., Pratt, G. W., Piffaretti, R., et al. 2010, A&A, 517, A92
- Bahcall, N. A., & Fan, X. 1998, ApJ, 504, 1
- Behroozi, P., Wechsler, R., Hearin, A., & Conroy, C. 2018, ArXiv e-prints, arXiv:1806.07893
- Behroozi, P., Wechsler, R., & Wu, H.-Y. 2012, Rockstar: Phase-space halo finder, Astrophysics Source Code Library, ascl:1210.008
- Bilton, L. E., & Pimblett, K. A. 2018, MNRAS, 481, 1507
- Biviano, A., Katgert, P., Thomas, T., & Adami, C. 2002, A&A, 387, 8
- Biviano, A., Murante, G., Borgani, S., et al. 2006, A&A, 456, 23
- Bocquet, S., Saro, A., Mohr, J. J., et al. 2015, ApJ, 799, 214
- Brodwin, M., Ruel, J., Ade, P. A. R., et al. 2010, ApJ, 721, 90
- Caldwell, C. E., McCarthy, I. G., Baldry, I. K., et al. 2016, MNRAS, 462, 4117
- Comparat, J., Prada, F., Yepes, G., & Klypin, A. 2017, MNRAS, 469, 4157
- de Haan, T., Benson, B. A., Bleem, L. E., et al. 2016, ApJ, 832, 95
- DES Collaboration, Abbott, T. M. C., Abdalla, F. B., et al. 2017, ArXiv e-prints, arXiv:1708.01530
- Eddington, A. S. 1913, MNRAS, 73, 359
- Evrard, A. E., Bialek, J., Busha, M., et al. 2008, Astrophys.J., 672, 122
- Farahi, A., Evrard, A. E., McCarthy, I., Barnes, D. J., & Kay, S. T. 2018, MNRAS, 478, 2618
- Gifford, D., Miller, C., & Kern, N. 2013, ApJ, 773, 116
- Goto, T. 2005, MNRAS, 359, 1415

- Hartlap, J., Simon, P., & Schneider, P. 2007, *A&A*, 464, 399
- Heymans, C., Grocutt, E., Heavens, A., et al. 2013, *MNRAS*, 432, 2433
- Hildebrandt, H., Viola, M., Heymans, C., et al. 2017, *MNRAS*, 465, 1454
- Hildebrandt, H., Köhlinger, F., van den Busch, J. L., et al. 2018, arXiv e-prints, arXiv:1812.06076
- Hill, J. C., Sherwin, B. D., Smith, K. M., et al. 2014, ArXiv e-prints, arXiv:1411.8004
- Klypin, A., Yepes, G., Gottlöber, S., Prada, F., & Heß, S. 2016, *MNRAS*, 457, 4340
- Lau, E. T., Nagai, D., & Kravtsov, A. V. 2010, *ApJ*, 708, 1419
- Leauthaud, A., Saito, S., Hilbert, S., et al. 2017, *MNRAS*, 467, 3024
- Lin, W., & Ishak, M. 2017, ArXiv e-prints, arXiv:1708.09813
- Mantz, A. B., von der Linden, A., Allen, S. W., et al. 2015, *MNRAS*, 446, 2205
- Ntampaka, M., Trac, H., Cisewski, J., & Price, L. C. 2017, *ApJ*, 835, 106
- Okoli, C., & Afshordi, N. 2016, *MNRAS*, 456, 3068
- Owers, M. S., Allen, J. T., Baldry, I., et al. 2017, *MNRAS*, 468, 1824
- Percival, W. J., Ross, A. J., Sánchez, A. G., et al. 2014, *MNRAS*, 439, 2531
- Pierre, M., Valotti, A., Faccioli, L., et al. 2017, *A&A*, 607, A123
- Planck Collaboration, Ade, P. A. R., Aghanim, N., et al. 2014a, *A&A*, 571, A16
- . 2014b, *A&A*, 571, A20
- . 2014c, *A&A*, 571, A29
- . 2016a, *A&A*, 594, A13
- . 2016b, *A&A*, 594, A24
- Planck Collaboration, Aghanim, N., Akrami, Y., et al. 2018, arXiv e-prints, arXiv:1807.06209
- Rines, K., Geller, M. J., & Diaferio, A. 2010, *ApJL*, 715, L180
- Rines, K., Geller, M. J., Diaferio, A., & Kurtz, M. J. 2013, *ApJ*, 767, 15
- Rines, K. J., Geller, M. J., Diaferio, A., & Hwang, H. S. 2016, *ApJ*, 819, 63
- Ruel, J., Bazin, G., Bayliss, M., et al. 2014, *ApJ*, 792, 45
- Saro, A., Mohr, J. J., Bazin, G., & Dolag, K. 2013, *ApJ*, 772, 47
- Schaye, J., Crain, R. A., Bower, R. G., et al. 2015, *MNRAS*, 446, 521
- Sifón, C., Menanteau, F., Hasselfield, M., et al. 2013, *ApJ*, 772, 25
- Taylor, A., Joachimi, B., & Kitching, T. 2013, *MNRAS*, 432, 1928
- Tinker, J., Kravtsov, A. V., Klypin, A., et al. 2008, *ApJ*, 688, 709
- Wilson, M. J., Sherwin, B. D., Hill, J. C., et al. 2012, *PhRvD*, 86, 122005
- Wu, H.-Y., Hahn, O., Evrard, A. E., Wechsler, R. H., & Dolag, K. 2013, *MNRAS*, 436, 460
- Zwicky, F. 1933, *Helvetica Physica Acta*, 6, 110